Impairment of sugar transport in the vascular system acts on nitrogen remobilisation and nitrogen use efficiency in Arabidopsis.

Authors: Beate Hoffmann[1], Emilie Aubry[1], Anne Marmagne[1], Sylvie Dinant[1], Fabien Chardon[1] and Rozenn Le Hir[1,*]

Affiliations

[1] Université Paris-Saclay, INRAE, AgroParisTech, Institut Jean-Pierre Bourgin (IJPB), 78000, Versailles, France

*** Corresponding author:** Dr R. Le Hir
Telephone: +33 1 30 83 36 56
Fax: +33 1 30 83 30 96
rozenn.le-hir@inrae.fr
ORCID ID : 0000-0001-6076-5863

Co-authors email addresses:
Beate Hoffmann: beate.hoffmann@inrae.fr
Emilie Aubry: emilia.aubry@orange.fr
Anne Marmagne : anne.marmagne@inrae.fr
Fabien Chardon : fabien.chardon@inrae.fr
Sylvie Dinant : sylvie.dinant@inrae.fr

Submission date : 14/09/2022

Number of figures: 6
Number of tables: 1
Word count: 5801 words
Number of supplementary figures: 5

Running title: Establishing a link between sugar transport, NUE and NRE

Abstract

The carbon (C) and nitrogen (N) metabolisms have long been known to be coupled, and this is required for adjusting nitrogen use efficiency. Despite this intricate relationship, it is still unclear how a deregulation of sugar transport impacts N allocation. Here we investigated, in Arabidopsis, the consequences of the simultaneous downregulation of the genes coding for the sugar transporters *SWEET11*, *SWEET12*, *SWEET16,* and *SWEET17* genes on various anatomical and physiological traits ranging from the stem's vascular system development, plant biomass production, seed yield, and N remobilisation and use efficiency. Our results show that intracellular sugar exchanges mediated by SWEET16 and SWEET17 proteins specifically impact the vascular development but do not play a significant role in the distribution of N. Most importantly, we showed that the double mutant *swt11swt12*, which is also impacted in the vascular development, displays an improved nitrogen use efficiency and nitrogen remobilisation to the seeds. In addition, a significant negative correlation between sugar and amino acids contents and the inflorescence stem radial growth exists, highlighting the complex interaction between the maintenance of C/N homeostasis and the inflorescence stem development. Our results thus deepen the link between sugar transport, C/N allocation and vascular system development.

Highlight: The disruption of genes coding for SWEET11 and SWEET12 sugar transporters negatively impacts the stem development but improves the plant nitrogen use efficiency and nitrogen remobilisation to the seeds.

Keywords: SWEET transporters, vascular system, xylem, stem, NUE, NRE, sugars, amino acids.

Introduction

Carbon (C) and nitrogen (N) are essential and limiting elements for plant, animal, and microorganism growth. In plants, the tricarboxylic acid (TCA) cycle is the primary source of C skeletons required for ammonium assimilation and is linked to the amino acid metabolism by the glutamate dehydrogenase, thus bridging C and N metabolisms (Huppe and Turpin, 1994; Hodges, 2002). In addition, N plays a significant role in C metabolism due to its function in Rubisco synthesis. At the same time, C compounds are essential for N absorption, nitrate reduction, N_2 fixation, and amino acid metabolism to generate C skeletons, metabolic energy, and reductants (Baslam *et al.*, 2021). To successfully reproduce, plants must constantly adjust their C and N contents. Such modulation can be achieved at various levels of control, ranging from the modulation of nutrient assimilation proteins' activity and the control of nutrient transport to a variety of mechanisms controlling the expression of genes encoding the proteins involved in nutrient metabolism, transport, and signaling. This has been exemplified in many studies which focused on improving C/N metabolism and transport to reach higher plant yield (Braun *et al.*, 2014; The *et al.*, 2021; Marmagne *et al.*, 2022).

To reach the seeds, sugars and amino acids, the primary products of C and N metabolisms, are transported through the vasculature (i.e., xylem and phloem) (van Bel, 2021). It is now well established that the main C pools are delivered long distance from the phloem, whereas the N pools are provided from both xylem and phloem. A third significant transport pathway is the lateral transfer of sugars and amino acids between phloem and xylem and *vice versa* (Tegeder and Masclaux-Daubresse, 2018; Aubry *et al.*, 2019). To ensure an appropriate distribution of sugars and amino acids at the whole plant level, nutrients can move through the plasmodesmata (symplasmic pathway), even if experimental proof of such a transport pathway for amino acids is still lacking (Kim *et al.*, 2021*a*), or by specialised transporters (e.g. SUGAR WILL EVENTUALLY BE EXPORTED TRANSPORTERS (SWEET), USUALLY MULTIPLE ACIDS MOVE IN AND OUT TRANSPORTERS (UmamiTs), SUCROSE TRANSPORTERS (SUC), and the AMINO ACID PERMEASES (AAPs) (Ladwig *et al.*, 2012; Müller *et al.*, 2015; Tegeder and Masclaux-Daubresse, 2018; Xue *et al.*, 2022). Overall, the delivery of nutrients from cell to cell and long-distance encompasses an intricate network between the metabolism products and their transport pathways that *in fine* creates source (e.g. leaves and stems) and sink organs (e.g. seeds, roots). The functional characterisation of these specialised transporters proteins shows that they are expressed in different plant organs (roots, leaves, stem, seeds), tissues (xylem, phloem, parenchyma cells, mesophyll cells) and

60 subcellular compartment (plasma membrane or tonoplast), suggesting that tight coordination of
61 their transport activities is needed for every step of plant development and growth. In this
62 respect, genetic modifications have been used to understand the contributory role of sugar and
63 amino acid transporter genes in increasing the C and N nutrition of seeds in crop and non-crop
64 species (Wingenter *et al.*, 2010; Zhang *et al.*, 2010; Lu *et al.*, 2020; Grant *et al.*, 2021). For
65 instance, the concurrent overexpression of amino acid permease AAP1 and sucrose transporter
66 SUT1 in pea increased the nutrient fluxes from source to sink, resulting in increased seed
67 number and protein content (Grant *et al.*, 2021). Nonetheless, despite the need to develop new
68 strategies to improve plant yield and quality, experimental data regarding the impact of
69 deregulation of sugar transport on N allocation or amino acids transport on C allocation is still
70 scarce (Perchlik and Tegeder, 2018; Lu *et al.*, 2020).
71 In this work, we proposed to fill this gap by evaluating consequences of a deregulation
72 of members of the SWEET sugar transporter family on biomass production, seed yield and N
73 allocation in Arabidopsis. Based on our previous work, we focused on the concurrent
74 downregulation of *SWEET11*, *SWEET12*, *SWEET16* and *SWEET17* genes shown to be
75 expressed in the inflorescence stem (Le Hir *et al.*, 2015; Aubry *et al.*, 2022). Indeed, this organ
76 constitutes an obligatory step for nutrients to be transported from leaves to seeds and is therefore
77 of interest when studying whole plant C and N allocation. Overall, the analysis of the
78 *swt11swt12, swt16swt17* double mutants and the *swt11swt12swt16swt17* quadruple mutant
79 allowed us to establish a link between the sugar transport between the different vascular cell
80 types, nitrogen use efficiency (NUE) and nitrogen remobilisation to the seeds (NRE).
81

82 **Materials and Methods**

83 *Plant material and growth conditions*

84 In order to obtain the quadruple mutant *sweet11-1sweet12-1sweet16-4sweet17* (hereafter
85 referred as *swt-q*), we crossed the *sweet11-1sweet12-1* (hereafter referred as *swt11swt12*)
86 double mutant (Le Hir *et al.*, 2015) with the *sweet16-4sweet17-1* (hereafter referred as
87 *swt16swt17*) double mutant (Aubry *et al.*, 2022). Homozygous plants were genotyped using
88 gene-specific primers in combination with a specific primer for the left border of the T-DNA
89 insertion (Supplementary Table S1). By using RT-PCR analysis, we confirmed that full length
90 transcripts of *SWEET11*, *SWEET12*, *SWEET16* and *SWEET17* cannot be amplified in the *swt-*
91 *q* mutant line (Supplementary Fig. S1 and Supplementary Table S1 for primers sequences). To
92 synchronize germination, seeds were stratified at 4°C for 48 hours and sown in soil in a growth

93 chamber in long day conditions (16 hours day/8 hours night and 150 µE m^{-2} s^{-1}) at 22/18°C
94 (day/night temperature) with 35% relative humidity. Plants were watered with PlantProd
95 nutrient solution twice a week (Fertil, https://www.fertil.fr/).
96
97 *GUS staining*
98 The lines expressing pSWEET11:SWEET11-GUS or pSWEET12:SWEET12-GUS
99 (Chen *et al.*, 2012) and pSWEET16:SWEET16-GUS or pSWEET17:SWEET17-GUS (Guo *et*
100 *al.*, 2014) in Col-0 background were used to assess SWEET11, SWEET12, SWEET16 and
101 SWEET17 expression pattern on seven-week-old plants grown in the greenhouse. The
102 histochemical GUS staining was performed according to Sorin et al. (2005). Inflorescence
103 stems subjected to GUS staining were then embedded in 8% (w/v) agarose and sectioned with
104 a Leica VT100S vibratome (Leica, https://www.leica-microsystems.com/). Sections were
105 counterstained for lignin by phloroglucinol staining (Pradhan Mitra and Loqué, 2014). Pictures
106 were taken using a Leitz Diaplan microscope equipped with an AxioCam MRc camera and the
107 ZEN (blue edition) software package (Zeiss, https://www.zeiss.com/).
108
109 *Inflorescence stem growth and sample preparation*
110 The main inflorescence stem height was measured with a ruler at 45 days after sowing
111 (DAS) and the stem diameter was measured either on Image J with the Feret diameter tool (see
112 next paragraph) or with a digital caliper at the bottom of the stem. At 45 DAS, 1 to 2 cm segment
113 was taken at the bottom part of the stem. Stem segments were embedded in 8% agarose solution
114 and sectioned with a VT100 S vibratome (Leica, https://www.leica-microsystems.com/). Cross-
115 sections were stained with a FASGA staining solution prepared as described in Tolivia and
116 Tolivia (1987) for morphometric analysis of the different stem tissues.
117
118 *Morphometric analysis of the stem tissues*
119 Stained inflorescence stem cross-sections were imaged under an Axio Zoom V16
120 microscope equipped with a Plan-Neofluar Z 2.3/0.57 FWD 10.6 objective (Zeiss,
121 https://www.zeiss.fr/microscopie/). For each section, several parameters were measured: stem
122 diameter, stem area, vascular system area (combining the area of all the vascular bundles), pith
123 area, the phloem area (combining the phloem area of all vascular bundles), the xylem area
124 (combining the xylem area of all vascular bundles) and the interfascicular thickness. The area
125 of the other tissues (including epidermis, cortex and interfascicular fibres) was then calculated

126 by subtracting the sum of the pith, phloem and xylem areas to the stem area. All parameters
127 were measured using the Image J software package (https://imagej.nih.gov/ij/). For the same
128 sections all the vascular bundles (VBs) were photographed individually using a confocal laser
129 scanning microscope and morphological analysis of the xylem were performed as described in
130 Le Hir et al. (2015). For each VB, the morphological segmentation allowed to access to the
131 number of xylem cells (xylary fibres and xylem vessels) as well as their cross-sectional areas.
132 Cells with a cross-sectional area comprised between 5 to 150 μm^2 were considered to be xylary
133 fibres and cells with a cross-sectional area greater than 150 μm^2 were considered to be xylem
134 vessels. The sum of all xylem cell cross-sectional areas was then calculated to give the total
135 xylem cross-sectional area. The average xylary fiber and xylem vessel area was calculated by
136 dividing the total xylem cross-sectional area by the number of each cell type.
137
138 *Quantification of soluble sugars, starch and total amino acids*
139 Main inflorescence stems of wild type, *swt11swt12*, *swt16swt17* and *swt-q* mutants,
140 without lateral stems, siliques and flowers, were harvested in the middle of the day (8 hours
141 after the beginning in the light period), frozen in liquid nitrogen and ground with a mortar and
142 a pestle. Soluble sugars and starch were extracted from 50 mg of powder from an individual
143 stem and quantified by enzymatic method as described in Sellami et al. (2019). Total amino
144 acids quantification was performed according to the protocol of Rosen (1957) and using
145 Glutamine as a standard. Nine biological replicates coming from two independent experiments
146 were analysed.
147
148 *Nitrogen and carbon percentage measurement and ^{15}N labeling experiment*
149 The different genotypes were grown in a growth chamber as described above. Around 30
150 DAS, while plants are still at the vegetative stage, 1 ml of a 10 mM nitrate solution containing
151 10% of $^{15}NO_3$ was applied on the soil close to the plants collar. Then, plants were let to grow
152 until the end of their cycle and harvested once all seeds were matured and the rosette dried.
153 Plants were separated in different samples: (i) rosette, (ii) stem (including the main and lateral
154 stems, cauline leaves and empty dry siliques), and seeds (total seeds). As plants were grown in
155 soil, we could not harvest the roots without losing a large part of them. The dry weight of the
156 different samples was determined. Then samples were ground to an homogenous fine powder
157 and a subsample of 1000 to 2000 µg was precisely weighted in tin capsules to determine the C
158 and N percentages (C% and N%) and the ^{15}N abundance using an elemental analyzer (FLASH

159 2000 Organic Elemental Analyzer, Thermo Fisher Scientific, Courtaboeuf, France) coupled to
160 an isotope ratio mass spectrometer (delta V isotope ratio mass spectrometer, Thermo Fisher
161 Scientific, Courtaboeuf, France) calibrated using international reference (caffeine, IAEA-600,
162 Vienna, Austria). The ^{15}N abundance along with the following parameters: Harvest Index (HI),
163 N allocation in rosette, N allocation in stem, N allocation in seeds (NHI), Nitrogen Use
164 Efficiency (NUE = NHI/HI), ^{15}N allocation in rosette, ^{15}N allocation in stem, ^{15}N allocation in
165 seeds (^{15}NHI) and Nitrogen Remobilisation Efficiency (NRE) were calculated as described
166 previously (Jasinski *et al.*, 2021). The NRE index is calculated as the ratio between the ^{15}NHI
167 (percentage of ^{15}N in seeds) over the plant HI (NRE = $^{15}NHI/HI$). Finally, the proportion of N
168 coming from remobilisation or post-flowering uptake was calculated as described in Marmagne
169 et al. (2022). The absolute quantity of C contained in each sample was defined as QtyC = DW
170 x C%. The following formulas were then used to evaluate the parameters related to the C fluxes:
171
172 $$\text{C allocation in rosette} = QtyC_{rosette}/(QtyC_{rosette}+QtyC_{stem}+QtyC_{seeds})$$
173
174 $$\text{C allocation in stem} = QtyC_{stem}/(QtyC_{rosette}+QtyC_{stem}+QtyC_{seeds})$$
175
176 $$\text{C allocation in seeds} = QtyC_{seeds}/(QtyC_{rosette}+QtyC_{stem}+QtyC_{seeds})$$
177
178 *RNA isolation, cDNA synthesis and RT-PCR*
179 RNAs were prepared from the main inflorescence stem from 7-week-old plants grown as
180 described above. Samples were frozen in liquid nitrogen before being ground with a mortar and
181 a pestle. Powders were stored at -80°C until use. Total RNA was extracted from frozen tissue
182 using TRIzol® reagent (Thermo Fisher Scientific, 15595-026, https://www.thermofisher.com)
183 and treated with DNase I, RNase-free (Thermo Fisher Scientific, EN0521,
184 https://www.thermofisher.com). cDNA was synthetized by reverse transcribing 1 µg of total
185 RNA using RevertAid H minus reverse transcriptase (Thermo Fisher Scientific, EP0452,
186 https://www.thermofisher.com) with 1 µl of oligo(dT)18 primer (100 pmoles) according to the
187 manufacturer's instructions. The reaction was stopped by incubation at 70 °C for 10 min. Full-
188 length PCR was performed by using primers spanning the complete CDS for each gene tested
189 (Supplementary Table 1).
190
191 *Statistical analysis*

192 One-way ANOVA combined with a Tukey's comparison post-test was done using R
193 (version 4.0.2) and Rstudio (version 1.4.1103) software. A *P*-value <0.05 was considered as
194 significant. Spearman correlations were realized using R with adjusted p-values calculated with
195 the Holm's method. Principal component analysis was performed using the 'FactoMineR'
196 package of R (Le *et al.*, 2008). The least-square means were calculated using the R package
197 'emmeans'.
198
199 **Results**

200 It is now established that modifications of the facilitated transport of sugar at the plasma
201 membrane or the tonoplast lead to defects in the Arabidopsis shoot and root development (for
202 review see Xue *et al.*, 2022). However, to what extent perturbations of sugar exchanges at both
203 the plasma membrane and the tonoplast lead to defects in the plant growth and development
204 still needs to be explored. To address this question, we produced and characterised the
205 *swt11swt12swt16swt17* quadruple mutant (*swt-q*) along the corresponding *swt11swt12*,
206 *swt16swt17* double mutant lines (Le Hir *et al.*, 2015; Aubry *et al.*, 2022).

207 *The inflorescence stem growth and development are affected in quadruple sweet mutant line*
208 Alike *swt11swt12*, the inflorescence stem of *swt-q* was shorter and thinner (by about 30%)
209 than wild-type stem (Fig. 1A-C). Moreover, as previously described the stem of the *swt16swt17*
210 was thinner but not shorter than that of the wild type (Fig. 1A-C) (Aubry *et al.*, 2022). The stem
211 height to stem diameter ratio of both double mutants and the *swt-q* mutant was similar to that
212 of the wild-type plants (Fig. 1D).
213 We further characterised the inflorescence stem growth and measured after 45 days after
214 sowing the portions of the stem corresponding to the cauline leaf zone, and to the "true
215 inflorescence" (Pouteau and Albertini, 2009), the number of siliques, the density of siliques,
216 and the number of lateral inflorescences (Fig. 1E-H). We observed that, in wild-type plants, the
217 zone which carries the cauline leaves and the lateral inflorescence stems represents about 35%
218 of the total inflorescence stem height while about 65% is occupied by the true inflorescence
219 zone (Fig. 1E). Interestingly we observed that the proportion of this latter is reduced in the
220 *swt11swt12* and *swt-q* mutants compared to wild-type plants (Fig. 1E). This phenotype is
221 accompanied by a reduced number of siliques in the same genotypes (Fig. 1F). Nonetheless,
222 the silique density was not significantly different between all genotypes studied (Fig. 1G).
223 Finally, we did not observe any differences in the number of lateral inflorescence stems in any
224 mutant lines compared to wild-type plants (Fig. 1H). We also explored the tissue distribution

225 within the stem cross-section by measuring the area occupied by the pith, phloem, xylem and
226 outer tissues (i.e. epidermis, cortex and interfascicular fibres) as well as the thickness of the
227 interfascicular fibres (Fig. 1I-J). In our growth conditions, the pith represents about 47% of the
228 wild-type stem cross-sectional area while 14 % is occupied by the vascular system (phloem and
229 xylem). Finally, 39% of the total stem area is occupied by the epidermis, cortex and
230 interfascicular fibres. The results are in accordance with those previously published by Paul-
231 Victor and Rowe (2011). Interestingly the tissue organization changed in the different mutant
232 lines (Fig. 1I). Indeed, a significant decrease of the proportion of xylem tissue was measured in
233 the *swt-q* mutant compared to the wild type while no change in the proportion of phloem tissue
234 was measured in any of the lines (Fig. 1I). Moreover, a decreased proportion of pith tissue along
235 with an increased proportion of the outer tissue layers was measured in the *swt11swt12* and *swt-*
236 *q* mutants. Additionally, the thickness of the interfascicular fibres was significantly smaller in
237 all the mutant lines compared to the wild type (Fig. 1J). Therefore, the stem radial growth
238 phenotype could be associated to a defect in the stem tissue distribution with less xylem, pith
239 and interfascicular fibres.
240 Altogether these results show that both *swt11swt12* and quadruple mutants display similar
241 phenotype, suggesting that adding perturbations of the cytosol-vacuole sugar exchanges (*via*
242 disruption of the *SWEET16* and *SWEET17* expression) does not further affect the main
243 inflorescence stem growth and development.
244
245 *Interplay between stem growth parameters and nutrient content*
246 Both *swt11swt12* and *swt16swt17* double mutants have been shown to accumulate sugars
247 in rosette leaves and inflorescence stem (Chen *et al.*, 2012; Gebauer *et al.*, 2017; Aubry *et al.*,
248 2022). Moreover, it has been demonstrated that the content of metabolites such as sucrose,
249 glutamine and starch is negatively correlated with rosette biomass production (Meyer *et al.*,
250 2007; Sulpice *et al.*, 2009). Here, we tested the correlation between stem growth parameters
251 and stem nutrient content in the different genotypes by measuring the main inflorescence stem
252 diameter and height along with the total soluble sugars (sucrose, glucose and fructose), starch,
253 and total amino acids content on the same samples (Figs. 1 and 2). A significant increase of
254 soluble sugars, starch and amino acids contents was measured in the *swt11swt12* and *swt-q*
255 mutant lines compared to wild-type (Fig. 2). Additionally, we show that *swt16swt17* stems tends
256 to accumulate more soluble sugars compared to wild-type stems (Fig. 2). We then computed
257 correlation coefficients between these parameters (Table 1). Interestingly, a negative

258 correlation was shown between the inflorescence stem diameter/height and the total amino acids
259 content as well as between the stem diameter and the soluble sugars and starch contents (Table
260 1). Additionally, a positive correlation between inflorescence stem height and diameter as well
261 as a positive correlation between soluble sugars and starch contents were calculated (Table 1).
262 These results suggest that the SWEET-dependent stem radial growth phenotype is associated
263 with sugar and amino acid contents in this organ.
264
265 *Plant biomass production and seed yield are impaired in sweet mutant lines*
266 Up to now, effects of down or up-regulation of *SWEET11*, *SWEET12*, *SWEET16* and/or
267 *SWEET17* have been observed at an organ-specific level in rosette, stem, root or seeds (Chen
268 *et al.*, 2012, 2015; Chardon *et al.*, 2013; Klemens *et al.*, 2013; Guo *et al.*, 2014; Le Hir *et al.*,
269 2015; Valifard *et al.*, 2021; Aubry *et al.*, 2022). Here, we wanted to obtain a more
270 comprehensive view of the consequences of mutation in these genes on the aboveground organs
271 at the end of the plant development. For that purpose, the biomass produced by rosette leaves,
272 stem (including the main, lateral, secondary stems and the siliques envelopes) and seeds were
273 assessed along with the analysis of C and N contents in each organ (Fig. 3). Consistently with
274 previous report (Chen *et al.*, 2012), we show that rosette dry weight (DW) is significantly
275 reduced in the *swt11swt12* double mutant compared to the wild type by about 45% (Fig. 3A).
276 The same decrease in rosette biomass is observed for the *swt-q* mutant while no significant
277 effect of mutation in *SWEET16* and *SWEET17* is measured (Fig. 3A). Interestingly a significant
278 gain of biomass (about 40%) is measured only in the stem of the *swt16swt17* double mutant
279 (Fig. 3A). Consistently with fewer siliques (Fig. 1F), the seed yield was reduced in both
280 *swt11swt12* and *swt-q* mutant compared to wild-type plants (Fig. 3A). We also estimated the C
281 and N allocated to each organ in the 4 genotypes. In wild-type plants, N was allocated at 6%,
282 37%, and 57% to rosette, stem, and seeds respectively (Fig. 3B). In *swt11swt12* and *swt-q*
283 mutants, the N distribution was modified in all organs tested, with a significant decrease of N
284 allocation in rosette and seeds while a significant increase of N allocation in the stem in both
285 genotypes (Fig. 3B). C was allocated at 3.5%, 33% and 63.5% to rosette, stem and seeds
286 respectively in wild-type plants (Fig. 3C). A significant decrease in C distribution was measured
287 in the seeds of the *swt11swt12* and *swt-q* mutants while a significant increase of C was allocated
288 to their stem (Fig. 3C). Finally, the *swt16swt17* double mutant displayed an intermediate
289 phenotype for N and C allocation between WT and the other mutants (*swt11swt12* and *swt-q*)
290 but no statistical difference was measured compared to the wild type.

291 We also estimated the harvest index (HI) which corresponds to the ratio of seeds DW to
292 aboveground plant DW at harvest time. In our growth conditions, HI represents about 50% in
293 wild-type plants (Fig. 3D). It was significantly lower (by about 70%) in the *swt11swt12* and
294 *swt-q* mutants while no significant difference was observed for the *swt16swt17* mutant
295 compared to the wild type albeit a similar tendency (Fig. 3D). Since the *swt11swt12* and *swt-q*
296 mutants produce less seeds (lower HI) with a lower proportion of N in seeds (lower NHI), we
297 determined the Nitrogen Use Efficiency (NUE) as the ratio of Nitrogen Harvest Index (NHI)-
298 to-Harvest Index (HI) to have information about the efficiency of the different lines to store N
299 in seeds irrespective of the plant capacity to produced seeds. Interestingly, we measured an
300 improved NUE in the *swt11swt12* and *swt-q* mutants compared to the wild type and the
301 *swt16swt17* mutant (Fig. 3E). This suggest that *SWEET11* and *SWEET12* negatively impact the
302 way the plant is efficiently using its nitrogen. Finally, we estimated the seed composition in the
303 different genotypes and observed a significant decrease in the C percentage while the N
304 percentage was significantly increased in the *swt11swt12* and quadruple mutants (Fig. 3F-G).
305 As a consequence, the C:N ratio of the seeds was significantly decreased in both genotypes
306 (Fig. 3H).
307
308 *Mutation in SWEET genes affects N remobilisation efficiency*
309 Despite an improved NUE in the *swt11swt12* mutant, we observed a decreased C and N
310 allocation to seeds in this genotype (Fig. 3B, C and E). In order to understand in which organ,
311 the N flux might be blocked, we analysed the ^{15}N partitioning to rosette, stem and seeds in the
312 different mutants (Fig. 4). The use of ^{15}N labeling allows to estimate the plant capacity to
313 remobilize to the seeds the N compounds produced and stored in the rosette during the labeling
314 period (Marmagne *et al.*, 2020). In wild-type plants, 5% of ^{15}N remained in the rosette while
315 45% was stored in the stem, and 50% was remobilized to the seeds (Fig. 4A-C). Our results
316 show that, consistently with a better NUE, less ^{15}N remains in the rosette of the *swt11swt12*
317 mutant (Fig. 4A). A similar tendency, albeit not significant, was observed in *swt16wt17* and
318 quadruple mutants compared to wild-type plants (Fig. 4A). Interestingly, a significant increased
319 proportion of ^{15}N was measured in the stem of the *swt11swt12* and *swt-q* mutants (Fig. 4B)
320 which led to a lower ^{15}N remobilisation to the seeds (Fig. 4C). Finally, the calculation of the
321 NRE index allowed to determine if the ^{15}N partitioning to seeds is totally controlled by sink
322 strength. In both the *swt11swt12* and *swt-q* mutants, we observed a significant increase of the
323 NRE index compared to the wild-type plants (Fig. 4D). Altogether these results show that

324 disruption of *SWEET11* and *SWEET12* gene expression leads to better nitrogen use efficiency
325 and remobilisation efficiency from the rosette. However, the N remobilized from the rosette
326 accumulates in the stem at the expense of the seeds, most probably explaining the lower harvest
327 index.
328 The nitrogen presents in seeds is coming from both N remobilisation and post-flowering
329 N uptake by the roots. Based on the results of the ^{15}N labeling, we could also deduce the
330 proportion of both N origin in seeds (Marmagne *et al.*, 2022). In wild-type plants, about 60%
331 of N found in seeds is coming from the remobilisation process while the remaining 40% is
332 linked to the post-flowering N uptake (Fig. 4E). Interestingly, in the *swt11swt12* double mutant
333 and in the *swt-q* mutant, these proportions are severely impacted and the N part originated from
334 post-flowering uptake is strongly reduced (Fig. 4E). In the *swt16swt17* double mutant seeds,
335 the N coming from the post-flowering uptake is also slightly modified compared to wild-type
336 seeds but the difference is not statistically different (Fig. 4E). These results further strengthen
337 the existence of an association of sugar transport with N uptake and remobilisation to seeds.
338
339 *Quantitative analysis of the different vascular bundle types and impact of mutations in SWEET*
340 *genes*
341 Nitrate, and amino acids are mostly transported in the xylem sap from leaves to seeds
342 through the stem (Tegeder and Masclaux-Daubresse, 2018). Since we observed fewer xylem
343 tissues in the stem of mutant lines together with an improved nitrogen remobilisation, we further
344 explore the stem xylem defect by performing a quantitative analysis of the xylem in a vascular-
345 bundle type manner (Fig. 5, and Supplementary Figs. S2-S5). Indeed, three different VB types
346 can be observed in Arabidopsis stem: the M (main stem)-type VBs which are the most common
347 and are characterised by a triangular shape; the B (branch)-type VBs that are dividing VBs
348 connected to a lateral inflorescence stem; and the L (leaf)-type VBs that are round-shaped VBs
349 connected to the cauline leaf vasculature (Fig. 5A). The M-type and B-type correspond to VBs
350 involved in root-to-shoot transport of water and N derived nutrients to the seeds (Park *et al.*,
351 2015). In wild-type plants, we observed around 10 VBs among which between 4-6 M-type VBs,
352 2-3 B-type VBs and 2-3 L-type VBs (Fig. 5B). When the expression of *SWEET11* and
353 *SWEET12* is disrupted, no significant change in the total number of VBs is observed (Fig. 5B).
354 However, when the expression of both genes coding for the tonoplastic SWEET16 and
355 SWEET17 transporters is impaired, a significant decrease of the total number of VBs is
356 observed compared to the wild-type plants (Fig. 5B). Interestingly, in the *swt-q* mutant line,

357 similarly to the *swt16swt17* mutant, we also found fewer VBs compared to the wild-type plants
358 (Fig. 5B). While the same number of B-type VB is observed in the *swt16swt17* double mutant
359 compared to the wild type, significantly fewer M-type VBs and a tendency for more L-type
360 VBs are observed in this mutant line (Fig. 5B). In the *swt-q* mutant a trend, albeit not significant,
361 for less M-type and L-type VBs and more B-type VBs is observed (Fig. 5B).
362 Several anatomical parameters such as xylary fibres and xylem vessels numbers and sizes
363 were then measured to detail the morphological features of the different VB types. A principal
364 component analysis (PCA) was applied to the dataset obtained on wild-type plants and allowed
365 to observe a separation between the different VB types within the projection of the two first
366 principal component planes that gather more than 83% of the total variation (Supplementary
367 Fig. S2A). The first dimension clearly separates the B-type VB from the L-type VB while the
368 M-type VB present an intermediate phenotype (Supplementary Fig. S2A). The number of
369 xylem cells (xylary fibres and xylem vessels) and the area occupied by xylem vessels are the
370 factors which are contributing the most to this separation (Supplementary Fig. S2B). The data
371 show that B-type VBs are characterised by more and bigger xylary fibres than M-type VBs
372 (Supplementary Fig. S2B). L-type VBs display fewer and smaller xylem vessels as well as a
373 smaller fibre-to-vessel ratio than the M-type VBs (Supplementary Fig. S2B). In the mutant line,
374 independently of the VB type, the *swt11swt12* and *swt-q* mutant lines displayed significantly
375 fewer and smaller xylary fibres and xylem vessels (Fig. 5C and Supplementary Figs. 3, 4 and
376 5) compared to the wild type. Nonetheless, one exception is observed in the B-type VBs of the
377 *swt11swt12* double mutant for which no difference of the total number of vessels is observed
378 compared to the wild type (Supplementary Fig. 3C). In addition, we observe that, compared to
379 the wild type, *swt16swt17* double mutant displayed significantly fewer and smaller xylem cells
380 (including fibres and vessels) in M- and L-type VBs, but no significant effect was measured for
381 B-type VBs (Fig. 5C and Supplementary Figs. 3, 4 and 5).
382
383 SWEET11, SWEET12, SWEET16 *and* SWEET17 *have partially overlapping expression*
384 *pattern in the vascular tissues of the stem independently of the VB type*
385 Next the translational GUS fusions lines previously described (Chen *et al.*, 2012; Guo *et*
386 *al.*, 2014) were used to check the expression pattern of the different SWEET transporters in the
387 different VB types (Fig. 6). We observed that all four transporters are expressed both in phloem
388 and xylem whatever the VB type (Fig. 6). In the xylem tissue, SWEET11, SWEET16 and
389 SWEET17 are expressed in the developing xylem cells (Figure 6B, H and K) while an

390 expression of SWEET11, SWEET12 and SWEET17 is detected in the xylem parenchyma cells
391 located at the bottom of the vascular bundle in the protoxylem area (Fig. 6A-C, D-F and J-L).
392 This expression pattern is particularly visible in L-type VBs which are mainly composed of
393 parenchyma cells (Fig. 6C, F and L). In addition, SWEET11 and SWEET12 are localised in the
394 starch sheath cells, situated between the cortex and the phloem (Altamura *et al.*, 2001) (Fig.
395 6A-F). An expression of SWEET16 and SWEET17 is observed in the cortex cells and the
396 interfascicular fibers (Fig. 6G-L). Finally, SWEET17 is also expressed in some of the pith cells
397 (Fig. 6J-L).
398
399 **Discussion**
400 Modulation of inter or intracellular pool of sugars by modifying the expression of genes
401 involved in sugar metabolism or transport modifies shoot and root growth, and plant yield in
402 several species (e.g., Arabidopsis, Tomato, Tobacco, Poplar and Pea) (Dai *et al.*, 1999; Park *et*
403 *al.*, 2008; Wingenter *et al.*, 2010; Zhang *et al.*, 2010; Mahboubi *et al.*, 2013; Le Hir *et al.*, 2015;
404 Stein *et al.*, 2017; Lu *et al.*, 2020; Valifard *et al.*, 2021; Aubry *et al.*, 2022). However, the effect
405 of simultaneous disruption of sugar transport at both inter and intracellular levels has not been
406 explored so far. In this study we explored the effect on plant development and biomass
407 production of the disruption of two genes coding for proteins involved in intercellular sugar
408 transport, SWEET11, SWEET12, together with two genes coding for intracellular sugar
409 transporters, SWEET16 and SWEET17. *SWEET11* and *SWEET12* genes encode sugar
410 transporters located at the plasma membrane of vascular parenchyma cells in leaves and stem
411 (Chen *et al.*, 2012; Le Hir *et al.*, 2015; Cayla *et al.*, 2019; Kim *et al.*, 2021*b*). They were also
412 shown to be expressed in seeds and roots (Chen *et al.*, 2015; Desrut *et al.*, 2020). On the other
413 hand, *SWEET16* and *SWEET17* encode tonoplast-localized sugar transporters expressed in the
414 vascular system of leaves, stem and roots (Chardon *et al.*, 2013; Klemens *et al.*, 2013; Guo *et*
415 *al.*, 2014; Valifard *et al.*, 2021; Aubry *et al.*, 2022). Comparing the expression pattern of the
416 four SWEET transporters in inflorescence stem, we observed that they have partially
417 overlapping expression pattern in the phloem, the developing xylem cells and the xylem
418 parenchyma cells. In addition, SWEET11 and SWEET12 are expressed in endodermis-like cells
419 which transiently store starch (also called starch sheath cells) (Altamura *et al.*, 2001) and
420 SWEET16 and SWEET17 in the cortex cells. Interestingly the phenotype of the quadruple
421 mutant, for most of the traits related to plant biomass production and plant yield, is similar to
422 that of the *swt11swt12* double mutant. On the other hand, the phenotype of the *swt16sw17*

423 double mutant was similar to that of the wild type or intermediate between the *swt11swt12* and
424 *swt-q* mutants. These results suggest that intercellular facilitated transport of sugars, mediated
425 by SWEET11 and SWEET12, expressed conjointly in the starch sheath cells, the phloem and,
426 the xylem parenchyma, constitutes one limiting factor for plant biomass production and plant
427 yield. On the other hand, the maintenance of the sugar homeostasis within the cell, regulated
428 by SWEET16 and SWEET17 constitutes an important parameter for the regulation of the xylem
429 and interfascicular fibres development, consistently with their expression in these cell types
430 (Aubry *et al.*, 2022).

431 In Arabidopsis, the inflorescence stem results from two distinct morphogenetic
432 transitions, the so-called bolting transition and floral transition (Pouteau and Albertini, 2009).
433 The first part of the stem (cauline leaf zone), resulting from the bolting transition, is composed
434 of cauline leaves carrying an axillary flowering shoot while the "true inflorescence" carries the
435 flowers and siliques. Interestingly, we show that the reduction of inflorescence stem height in
436 the *swt11swt12* double mutant is mainly due to a specific decrease of the "true inflorescence"
437 height, suggesting that both transporters play a role in the floral transition. It is known that
438 during the floral transition, an increase of the sucrose in the phloem sap is required (Corbesier
439 *et al.*, 1998) and that the primary metabolism is reprogrammed including the transcriptional
440 activation of the gene coding for the sucrose transporter *SWEET10* by FLOWERING LOCUS
441 T (FT) transcription factor (Andrés *et al.*, 2020). Although a similar regulation of *SWEET11*
442 and *SWEET12* expression by FT is unlikely according to Andrés et al. (2020), the defect in the
443 sucrose phloem loading, previously observed in the source leaves of the *swt11swt12* double
444 mutant (Chen *et al.*, 2012) could account for this phenotype.

445 In the stem, we also show a perturbation of the C partitioning (including an accumulation
446 of soluble sugars and starch) along with an expression of both SWEET11 and SWEET12 in the
447 stem phloem tissue. These suggest that both transporters play a role in loading the phloem in
448 the stem as previously shown in leaves (Chen *et al.*, 2012). Moreover, our results show that in
449 stem they are also likely involved in the starch remobilisation from the starch sheath cells to
450 the phloem parenchyma cells. These results are in line with stems being a major contributor to
451 lifetime carbon gain during plant development (Earley *et al.*, 2009). Especially, it has been
452 shown that before the first siliques development, the main inflorescence stem store carbon such
453 as starch mainly in the endodermis-like cell layer above the phloem cells. Later in their
454 development, stems are re-exporting nutrients to sustain siliques development and seeds
455 maturation (Altamura *et al.*, 2001; Ohmae *et al.*, 2013; Sugita *et al.*, 2016; Durand *et al.*, 2018).

456 However, to which extent perturbations of the C allocation in stems impacts C percentage in
457 seeds is unclear. Part of the answer is provided by the C and N percentages in stems and seeds
458 obtained in Chardon et al. (2014) on an Arabidopsis RIL population. Interestingly, while seed
459 N% is positively correlated with stem N%, there is no significant correlation between seed C%
460 and stem C%. These results suggest that C remobilisation from the stem is much less important
461 for seed filling than the N remobilisation. Nonetheless, our results support that the lower C%
462 in seeds measured in the *swt11swt12* mutant could partially result from the overall defective
463 sugar loading in this mutant. This will lead to a decrease delivery of carbon to the seeds because
464 part of the C is not properly loaded or remobilized in the phloem sap from the stem and
465 accumulated as starch in this organ. In addition, both *SWEET11* and *SWEET12* together with
466 *SWEET15* have also been shown to be expressed in the different tissues of the seed (i.e.,
467 micropylar, endosperm and seed coat) across its development (Chen *et al.*, 2015). Consistently
468 *swt11swt12* and *swt11swt12swt15* mutant seeds display a decrease in their total fatty acid
469 content (Chen *et al.*, 2015). Therefore, the lower C% in the double mutant seeds could also be
470 the consequence of the defect in sugar transport within the different tissues of the seed. In the
471 future, a seed-specific complementation of the mutant phenotype could help to distinguish
472 between the contribution of the stem or seed in seed carbon allocation defect.

473 In agriculture, one of the dilemmas to solve in the near future consists in improving the
474 plant nitrogen use efficiency (NUE) to reduce production costs and environmental risks linked
475 to N leakage in the environment. While manipulating the expression of amino acid transporters
476 has been shown to efficiently improve NUE (Yang *et al.*, 2020), the effect of a deregulation of
477 sugar transporters on NUE is scarce (Schofield *et al.*, 2009; Klemens *et al.*, 2013). This is
478 surprising since C availability is known to be strongly associated with NUE (Fernie *et al.*,
479 2020). In this study, we show that mutation in the expression of both *SWEET11* and *SWEET12*
480 impact the N allocation at the whole plant level. Indeed, we measured (i) an increase of amino
481 acids content in the stem, (ii) an increase of N partitioning to the stem concomitantly with a
482 decrease in the seeds and in the rosette leaves, and (iii) an increase of ^{15}N proportion in the stem
483 and decrease in the seeds. Ultimately, *swt11swt12* double mutant displays an improved NUE
484 and NRE despite a lower harvest index. Finally, *swt11swt12* seeds display a lower C:N ratio
485 which points to a non-proportional enhancement of nitrogen supply (higher N%). In seeds of
486 several species such as sunflower, rapeseed, soybean and Arabidopsis, both C and N
487 percentages are strongly correlated (Marmagne *et al.*, 2020). Up to now, three hypotheses have
488 been proposed to explain this phenomenon: (i) the dilution effect of the protein concentration

489 by the enhanced oil concentration and *vice versa*, (ii) the competition effect between C and N
490 metabolisms for energy, and (iii) the N availability effect which suggests that the local N
491 quantity and quality may affect the C and N metabolisms in siliques (Marmagne *et al.*, 2020).
492 In addition, we could also propose that the retention of C and N in *swt11swt12* stem could also
493 be responsible for this lower C:N ratio in seeds. In this context, a feedback mechanism
494 consisting in a better nitrogen remobilisation efficiency from the rosette leaves is used to
495 compensate for the partial retention of N in stem. Moreover, our results point out that the
496 *swt11swt12* double mutant also displays a defect in the post-flowering N uptake by the roots.
497 Interestingly, in Arabidopsis seedlings, Chen et al. (2016) identified that the regulation of the
498 expression of *SWEET11* and *SWEET12* by the shoot-to-root mobile transcription factor
499 ELONGATED HYPOTOCOL5 (HY5) is required to modulate the expression of the nitrate
500 transporter *NRT1.2* in roots. Our results support this model and further suggest that SWEET16
501 and SWEET17 could also be considered since the *swt-q* mutant displays a tendency towards a
502 further decrease in post-flowering N uptake albeit not significant. Consistently, *swt17* single
503 mutant showed defects in root growth and architecture (Valifard *et al.*, 2021) that could also
504 account for N uptake impairment since both traits are strongly linked (Kiba and Krapp, 2016).
505 Altogether our results suggest that a proper sugar phloem loading mediated by SWEET11 and
506 SWEET12 negatively impacts the way the plant is using and remobilising its nitrogen to the
507 seeds. However, to better apprehend the C and N fluxes in the different *swt* mutant lines, ^{13}C
508 and ^{15}N labelling studies together with phloem and xylem saps composition measurements
509 could be of interest.

510 To be transported at long-distance, nutrients largely rely on the plant vascular system.
511 Especially, the inflorescence stem constitutes the obligatory way for nutrients to be distributed
512 from rosette leaves to the seeds (van Bel, 2021). Consistently with our previous works on
513 *swt11swt12* and *swt16swt17* double mutant lines (Le Hir *et al.*, 2015; Aubry *et al.*, 2022), we
514 further show that the disruption of the expression of the four *SWEET* genes affects the vascular
515 system expansion and tissue distribution. Especially the stem diameter decrease is likely due to
516 the impaired development of cells undergoing important secondary cell wall formation (i.e.,
517 xylem and interfascicular fibers). As described in Park et al. (2015), three different types of VB
518 with distinct functional features regarding water and mineral transport can be found in
519 Arabidopsis stem. In this study, we show that the VB types also display distinct anatomical
520 features, consisting in different proportion of xylary fibres, xylem vessels and xylem
521 parenchyma cells. These observations suggest the existence of a genetic control of their

522 differentiation, which will most probably involved transcription factors responsible for the
523 xylem cell type differentiation together with hormone regulation (Schuetz *et al.*, 2012).
524 Nonetheless, since sugars have also been shown to affect xylem development (Aloni, 1987),
525 we hypothesize that changes in the sugar availability mediated by SWEET transporters, could
526 be at play in the VB type differentiation. In line with this hypothesis, a lower number of VBs,
527 mainly due to less M-type VBs, was found only in *swt16swt17* mutant, along with a modified
528 cellular morphology in the VBs involved in the connexion with the cauline leaves (L-type VB)
529 and those responsible for long-distance transport of water and nutrients (M-type VB) (Park *et*
530 *al.*, 2015). Overall, these results suggest a possible reduced capacity for water and nutrient
531 transport as well as reduced exchanges of these compounds between the stem and the cauline
532 leaves that should be further examined. Nonetheless, since the plant yield is not affected in this
533 mutant, it is likely that genetic compensation occurs to sustain normal seeds quantity and
534 quality. Therefore, the intracellular sugar fluxes mediated by SWEET16 and SWEET17
535 specifically affect the stem xylem development without impacting the plant yield in normal
536 growth conditions. It could be of interest to test if the same holds true when plants are grown
537 in limiting conditions such as osmotic stress for which xylem transport is important (Shafi *et*
538 *al.*, 2015; Shinohara *et al.*, 2019). On the other hand, the defect in the sugar
539 export/remobilisation capacity in the stem likely account for the global stem growth and
540 development phenotype observed in the *swt11swt12* double mutant. Then, the resulting
541 increased sugar storage in stem and leaves disturbs the plant capacity to deal with N and *in fine*
542 the plant yield.

543 Interestingly, a significant negative correlation was found between stem diameter and
544 nutrient contents (i.e. soluble sugars, starch and amino acids). Considering that stem diameter
545 and nutrient contents could account for xylem development and C/N allocation respectively,
546 our results support a link between both traits. A role for sugars in the vasculature development
547 has been proposed for long, even if the identification of molecular actors involved starts only
548 to emerge (for review Dinant and Le Hir, 2022). On the other hand, a similar role for amino
549 acids has not been explored so far. Nonetheless, in tree stem, a nitrogen addition, an increased
550 carbon allocation or, to a lesser extent phosphorus addition, promotes the enlargement of the
551 vascular system (Plavcová *et al.*, 2013; Cai *et al.*, 2017; Hacke *et al.*, 2017; Hartmann *et al.*,
552 2020). At the opposite, in sunflower root, a high root N has been associated with lower vessels
553 number and size in sunflower (Bowsher *et al.*, 2016). Thus, this organ-dependent relationship
554 between vascular development and C/N allocation highlights the complex interaction between

both traits. A higher complexity level must also be added since nutrients act both as energy-provider compounds and signal molecules (Fichtner *et al.*, 2021). Therefore, future studies exploring the link between nutrients allocation and vascular system development must consider a multiscale approach from tissue to whole plant level.

Supplementary data

The following supplementary data are available at JXB online.

Fig. S1. Molecular characterisation of the quadruple *sweet* mutant lines.
Fig. S2. Distinct morphological features of the different vascular bundle's type in wild-type stems.
Fig. S3. Cellular morphology of M-type pole in the different genotypes.
Fig. S4. Cellular morphology of B-type pole in the different genotypes.
Fig. S5. Cellular morphology of L-type pole in the different genotypes.
Table S1. Primers used for characterising the quadruple mutant line.

Acknowledgments

We thank Catherine Bellini for critical reading of the manuscript.

Authors contribution

Conceptualization, R.L.H.; investigation, B.H., E.A., A.M., F.C. and R.L.H.; methodology, B.H., E.A. and A.M.; visualization, S.D., F.C. and R.L.H.; writing—original draft, R.L.H.; writing—review and editing, S.D., F.C. and R.L.H.

Conflicts of interest

The authors declare that the research was conducted in the absence of any commercial or financial relationships that could be construed as a potential conflict of interest.

582 **Funding**

583 This work has benefited from the support of IJPB's Plant Observatory technological platforms
584 and from a French State grant (Saclay Plant Sciences, reference ANR-17-EUR-0007, EUR SPS-
585 GSR) managed by the French National Research Agency under an Investments for the Future
586 program (reference ANR-11-IDEX-0003-03) through PhD funding to E.A.
587

588 **Data availability**

589 The data supporting the findings of this study are available from the corresponding author,
590 Rozenn Le Hir, upon request.

591

References

Aloni R. 1987. Differentiation of vascular tissues. **38**, 179–204.

Altamura MM, Possenti M, Matteucci A, Baima S, Ruberti I, Morelli G. 2001. Development of the vascular system in the inflorescence stem of Arabidopsis. New Phytologist **151**, 381–389.

Andrés F, Kinoshita A, Kalluri N, *et al.* 2020. The sugar transporter SWEET10 acts downstream of FLOWERING LOCUS T during floral transition of Arabidopsis thaliana. BMC Plant Biology **20**, 1–14.

Aubry E, Dinant S, Vilaine F, Bellini C, Le Hir R. 2019. Lateral transport of organic and inorganic solutes. Plants **8**, 1–25.

Aubry E, Hoffmann B, Vilaine F, *et al.* 2022. A vacuolar hexose transport is required for xylem development in the inflorescence stem. Plant Physiology **188**, 1229–1247.

Baslam M, Mitsui T, Sueyoshi K, Ohyama T. 2021. Recent advances in carbon and nitrogen metabolism in C3 plants. International Journal of Molecular Sciences **22**, 1–39.

van Bel AJE. 2021. The plant axis as the command centre for (re)distribution of sucrose and amino acids. Journal of Plant Physiology **265**, 153488.

Bowsher AW, Mason CM, Goolsby EW, Donovan LA. 2016. Fine root tradeoffs between nitrogen concentration and xylem vessel traits preclude unified whole-plant resource strategies in Helianthus. Ecology and Evolution **6**, 1016–1031.

Braun DM, Wang L, Ruan YL. 2014. Understanding and manipulating sucrose phloem loading, unloading, metabolism, and signalling to enhance crop yield and food security. Journal

of Experimental Botany **65**, 1713–1735.

Cai Q, Ji C, Yan Z, Jiang X, Fang J. 2017. Anatomical responses of leaf and stem of Arabidopsis thaliana to nitrogen and phosphorus addition. Journal of Plant Research **130**, 1035–1045.

Cayla T, Le Hir R, Dinant S. 2019. *Live-Cell Imaging of Fluorescently Tagged Phloem Proteins with Confocal Microscopy*.

Chardon F, Bedu M, Calenge F, *et al.* 2013. Leaf fructose content is controlled by the vacuolar transporter SWEET17 in *Arabidopsis*. Current Biology **23**, 697–702.

Chardon F, Jasinski S, Durandet M, Lécureuil A, Soulay F, Bedu M, Guerche P, Masclaux-Daubresse C. 2014. QTL meta-analysis in Arabidopsis reveals an interaction between leaf senescence and resource allocation to seeds. Journal of experimental botany **65**, 3949–3962.

Chen L-Q, Lin IW, Qu X-Q, Sosso D, McFarlane HE, Londoño A, Samuels AL, Frommer WB. 2015. A Cascade of Sequentially Expressed Sucrose Transporters in the Seed Coat and Endosperm Provides Nutrition for the Arabidopsis Embryo. The Plant Cell **27**, 607–619.

Chen L-Q, Qu X-Q, Hou B-H, Sosso D, Osorio S, Fernie AR, Frommer WB. 2012. Sucrose efflux mediated by SWEET proteins as a key step for phloem transport. Science **335**, 207–211.

Chen X, Yao Q, Gao X, Jiang C, Harberd NP, Fu X. 2016. Shoot-to-Root Mobile Transcription Factor HY5 Coordinates Plant Carbon and Nitrogen Acquisition. Current Biology **26**, 640–646.

Corbesier L, Lejeune P, Bernier G. 1998. The role of carbohydrates in the induction of flowering in Arabidopsis thaliana: Comparison between the wild type and a starchless mutant. Planta **206**, 131–137.

Dai N, Schaffer A, Petreikov M, Shahak Y, Giller Y, Ratner K, Levine A, Granot D. 1999. Overexpression of Arabidopsis hexokinase in tomato plants inhibits growth, reduces photosynthesis, and induces rapid senescence. Plant Cell **11**, 1253–1266.

Desrut A, Moumen B, Thibault F, Le Hir R, Coutos-Thévenot P, Vriet C. 2020. Beneficial rhizobacteria Pseudomonas simia WCS417 induces major transcriptional changes in plant sugar transport. Journal of Experimental Botany **71**, 7301–7315.

Dinant S, Le Hir R. 2022. Delving deeper into the link between sugar transport, sugar signaling and vascular system development. Physiologia Plantarum **in press**.

Durand M, Mainson D, Porcheron B, Maurousset L, Lemoine R, Pourtau N. 2018. Carbon source–sink relationship in *Arabidopsis thaliana*: the role of sucrose transporters. Planta **247**,

587–611.

Earley EJ, Ingland B, Winkler J, Tonsor SJ. 2009. Inflorescences contribute more than rosettes to lifetime carbon gain in Arabidopsis thaliana (Brassicaceae). American Journal of Botany **96**, 786–792.

Fernie AR, Bachem CWB, Helariutta Y, *et al.* 2020. Synchronization of developmental, molecular and metabolic aspects of source–sink interactions. Nature Plants **6**, 55–66.

Fichtner F, Dissanayake IM, Lacombe B, Barbier F. 2021. Sugar and Nitrate Sensing: A Multi-Billion-Year Story. Trends in Plant Science **26**, 352–374.

Gebauer P, Korn M, Engelsdorf T, Sonnewald U, Koch C, Voll LM. 2017. Sugar Accumulation in Leaves of Arabidopsis sweet11/sweet12 Double Mutants Enhances Priming of the Salicylic Acid-Mediated Defense Response. Frontiers in Plant Science **8**, 1–13.

Grant JE, Ninan A, Cripps-Guazzone N, Shaw M, Song J, Petřík I, Novák O, Tegeder M, Jameson PE. 2021. Concurrent overexpression of amino acid permease AAP1 (3a) and SUT1 sucrose transporter in pea resulted in increased seed number and changed cytokinin and protein levels. Functional Plant Biology **48**, 889–904.

Guo W-J, Nagy R, Chen H-Y, Pfrunder S, Yu Y-C, Santelia D, Frommer WB, Martinoia E. 2014. SWEET17, a facilitative transporter, mediates fructose transport across the tonoplast of Arabidopsis roots and leaves. Plant Physiology **164**, 777–789.

Hacke UG, Spicer R, Schreiber SG, Plavcová L. 2017. An ecophysiological and developmental perspective on variation in vessel diameter. Plant Cell and Environment **40**, 831–845.

Hartmann H, Bahn M, Carbone M, Richardson AD. 2020. Plant carbon allocation in a changing world – challenges and progress: introduction to a Virtual Issue on carbon allocation: Introduction to a virtual issue on carbon allocation. New Phytologist **227**, 981–988.

Le Hir R, Spinner L, Klemens PAW, *et al.* 2015. Disruption of the sugar transporters AtSWEET11 and AtSWEET12 affects vascular development and freezing tolerance in Arabidopsis. Molecular Plant **8**, 1687–1690.

Hodges M. 2002. Enzyme redundancy and the importance of 2-oxoglutarate in plant ammonium assimilation. Journal of Experimental Botany **53**, 905–916.

Huppe HC, Turpin DH. 1994. Integration of carbon and nitrogen metabolism in plant and algal cells. Annual Review of Plant Physiology and Plant Molecular Biology **45**, 577–607.

Jasinski S, Fabrissin I, Masson A, Marmagne A, Lécureuil A, Bill L, Chardon F. 2021. ACCELERATED CELL DEATH 6 Acts on Natural Leaf Senescence and Nitrogen Fluxes in

Arabidopsis. Frontiers in Plant Science **11**, 1–15.

Kiba T, Krapp A. 2016. Plant nitrogen acquisition under low availability: Regulation of uptake and root architecture. Plant and Cell Physiology **57**, 707–714.

Kim J-Y, Loo EP-I, Pang TY, Lercher M, Frommer WB, Wudick MM. 2021*a*. Cellular export of sugars and amino acids: role in feeding other cells and organisms. Plant Physiology.

Kim J-Y, Symeonidi E, Pang TY, *et al.* 2021*b*. Distinct identities of leaf phloem cells revealed by single cell transcriptomics. The Plant Cell **33**, 511–530.

Klemens PAW, Patzke K, Deitmer J, Spinner L, Le Hir R, Bellini C, Bedu M, Chardon F, Krapp A, Neuhaus HE. 2013. Overexpression of the vacuolar sugar carrier *AtSWEET16* modifies germination, growth, and stress tolerance in Arabidopsis. Plant Physiology **163**, 1338–1352.

Ladwig F, Stahl M, Ludewig U, Hirner AA, Hammes UZ, Stadler R, Harter K, Koch W. 2012. Siliques Are Red1 from Arabidopsis Acts as a Bidirectional Amino Acid Transporter That Is Crucial for the Amino Acid Homeostasis of Siliques. Plant Physiology **158**, 1643–1655.

Le S, Josse J, Husson F. 2008. FactoMineR: An R package for multivariate analysis. Journal of Statistical Software **25**, 1–18.

Lu MZ, Snyder R, Grant J, Tegeder M. 2020. Manipulation of sucrose phloem and embryo loading affects pea leaf metabolism, carbon and nitrogen partitioning to sinks as well as seed storage pools. Plant Journal **101**, 217–236.

Mahboubi A, Ratke C, Gorzsás A, Kumar M, Mellerowicz EJ, Niittylä T. 2013. Aspen SUCROSE TRANSPORTER3 allocates carbon into wood fibers. Plant Physiology **163**, 1729–1740.

Marmagne A, Jansinski S, Fagard M, Bill L, Guerche P, Masclaux-Daubresse C, Chardon F. 2020. Post-flowering biotic and abiotic stresses impact nitrogen use efficiency and seed filling in Arabidopsis thaliana. Journal of Experimental Botany **71**, 4578–4590.

Marmagne A, Masclaux-Daubresse C, Chardon F. 2022. Modulation of plant nitrogen remobilization and post-flowering nitrogen uptake under environmental stresses. Journal of Plant Physiology **277**, 153781.

Meyer RC, Steinfath M, Lisec J, *et al.* 2007. The metabolic signature related to high plant growth rate in Arabidopsis thaliana. Proceedings of the National Academy of Sciences **104**, 4759–4764.

Müller B, Fastner A, Karmann J, *et al.* 2015. Amino acid export in developing arabidopsis seeds depends on UmamiT facilitators. Current Biology **25**, 3126–3131.

Ohmae Y, Hirose A, Sugita R, Tanoi K, Nakanishi TM. 2013. Carbon-14 labelled sucrose transportation in an *Arabidopsis thaliana* using an imaging plate and real time imaging system. Journal of Radioanalytical and Nuclear Chemistry **296**, 413–416.

Park JY, Canam T, Kang KY, Ellis DD, Mansfield SD. 2008. Over-expression of an arabidopsis family A sucrose phosphate synthase (SPS) gene alters plant growth and fibre development. Transgenic Research **17**, 181–192.

Park J, Kim HK, Ryu J, Ahn S, Lee SJ, Hwang I. 2015. Functional water flow pathways and hydraulic regulation in the xylem network of Arabidopsis. Plant and Cell Physiology **56**, 520–531.

Paul-Victor C, Rowe N. 2011. Effect of mechanical perturbation on the biomechanics, primary growth and secondary tissue development of inflorescence stems of Arabidopsis thaliana. Annals of Botany **107**, 209–218.

Perchlik M, Tegeder M. 2018. Leaf amino acid supply affects photosynthetic and plant nitrogen use efficiency under nitrogen stress. Plant Physiology **178**, 174–188.

Plavcová L, Hacke UG, Almeida-Rodriguez AM, Li E, Douglas CJ. 2013. Gene expression patterns underlying changes in xylem structure and function in response to increased nitrogen availability in hybrid poplar. Plant, Cell and Environment **36**, 186–199.

Pouteau S, Albertini C. 2009. The significance of bolting and floral transitions as indicators of reproductive phase change in Arabidopsis. Journal of Experimental Botany **60**, 3367–3377.

Pradhan Mitra P, Loqué D. 2014. Histochemical staining of Arabidopsis thaliana secondary cell wall elements. Journal of Visualized Experiments, 1–11.

Rosen H. 1957. A modified ninhydrin colorimetric analysis for amino acids. Archives of Biochemistry and Biophysics **67**, 10–15.

Schofield RA, Bi YM, Kant S, Rothstein SJ. 2009. Over-expression of STP13, a hexose transporter, improves plant growth and nitrogen use in Arabidopsis thaliana seedlings. Plant, Cell and Environment **32**, 271–285.

Schuetz M, Smith R, Ellis B. 2012. Xylem tissue specification, patterning, and differentiation mechanisms. Journal of Experimental Botany **64**, 11–31.

Sellami S, Le Hir R, Thorpe MR, Vilaine F, Wolff N, Brini F, Dinant S. 2019. Salinity effects on sugar homeostasis and vascular anatomy in the stem of the *Arabidopsis thaliana* inflorescence. International Journal of Molecular Sciences **20**, 3167.

Shafi A, Chauhan R, Gill T, Swarnkar MK, Sreenivasulu Y, Kumar S, Kumar N, Shankar R, Ahuja PS, Singh AK. 2015. Expression of SOD and APX genes positively regulates

secondary cell wall biosynthesis and promotes plant growth and yield in Arabidopsis under salt stress. Plant Molecular Biology **87**, 615–631.

Shinohara S, Okamoto T, Motose H, Takahashi T. 2019. Salt hypersensitivity is associated with excessive xylem development in a thermospermine-deficient mutant of Arabidopsis thaliana. Plant Journal **100**, 374–383.

Sorin C, Bussell JD, Camus I, *et al.* 2005. Auxin and light control of adventitious rooting in Arabidopsis require ARGONAUTE1. The Plant Cell Online **17**, 1343–1359.

Stein O, Avin-Wittenberg T, Krahnert I, Zemach H, Bogol V, Daron O, Aloni R, Fernie AR, Granot D. 2017. Arabidopsis fructokinases are important for seed oil accumulation and vascular development. Frontiers in Plant Science **7**, 1–16.

Sugita R, Kobayashi NI, Hirose A, Saito T, Iwata R, Tanoi K, Nakanishi TM. 2016. Visualization of uptake of mineral elements and the dynamics of photosynthates in Arabidopsis by a newly developed Real-Time Radioisotope Imaging System (RRIS). Plant and Cell Physiology **57**, 743–753.

Sulpice R, Pyl ET, Ishihara H, *et al.* 2009. Starch as a major integrator in the regulation of plant growth. Proceedings of the National Academy of Sciences of the United States of America **106**, 10348–10353.

Tegeder M, Masclaux-Daubresse C. 2018. Source and sink mechanisms of nitrogen transport and use. New Phytologist **217**, 35–53.

The SV, Snyder R, Tegeder M. 2021. Targeting Nitrogen Metabolism and Transport Processes to Improve Plant Nitrogen Use Efficiency. Frontiers in Plant Science **11**.

Tolivia D, Tolivia J. 1987. Fasga: A new polychromatic method for simultaneous and differential staining of plant tissues. Journal of Microscopy **148**, 113–117.

Valifard M, Le Hir R, Müller J, Scheuring D, Neuhaus HE, Pommerrenig B. 2021. Vacuolar fructose transporter SWEET17 is critical for root development and drought tolerance. Plant Physiology **187**, 2716–2730.

Wingenter K, Schulz A, Wormit A, Wic S, Trentmann O, Hoermiller II, Heyer AG, Marten I, Hedrich R, Neuhaus HE. 2010. Increased activity of the vacuolar monosaccharide transporter TMT1 alters cellular sugar partitioning, sugar signaling, and seed yield in Arabidopsis. Plant Physiology **154**, 665–677.

Xue X, Wang J, Shukla D, Cheung LS, Chen L-Q. 2022. When SWEETs Turn Tweens: Updates and Perspectives. Annual Review of Plant Biology **73**, 1–25.

Yang G, Wei Q, Huang H, Xia J. 2020. Amino acid transporters in plant cells: A brief review.

Plants **9**, 1–17.

Zhang L, Tan Q, Lee R, Trethewy A, Lee YH, Tegeder M. 2010. Altered xylem-phloem transfer of amino acids affects metabolism and leads to increased seed yield and oil content in Arabidopsis. The Plant Cell Online **22**, 3603–3620.

Table 1. Correlation matrix showing interrelationship between stem growth parameters and nutrients content. Spearman correlations with associated adjusted p-values calculated with the Holm's method (n= 40 observations).

Variables	Stem height	Stem diameter	Amino acids content	Soluble sugars content	Starch content
Stem height		0.69	-0.78	-0.29	0.03
Stem diameter	p<0.0001		-0.69	-0.51	-0.45
Amino acids content	p<0.0001	p<0.0001		0.49	0.13
Soluble sugars content	p=0.2033	p=0.0058	p=0.0071		0.49
Starch content	p=0.8356	p=0.0155	p=0.8158	p=0.0071	

Figure legends

Fig. 1. Main inflorescence growth and development is altered in the quadruple *sweet* mutant line. Photographs of a representative plant of wild-type, *swt11swt12*, *swt16swt17* and quadruple mutants taken at 45 DAS (A). Barplots showing the main inflorescence stem height (B), diameter (C) and the stem height-to-stem diameter ratio (D). Least-square means from three independent cultures ± SE (n=17 for each genotype). Letters indicate statistical difference between genotypes according to an ANOVA and Tukey's comparison post-test. Proportion of the stem occupied by the "cauline leaf zone" (CL zone) and the "true inflorescence zone" (Inflo zone) (E). Barplots showing the silique number (F), the silique density (G) and the number of lateral inflorescence stems (H). Stacked barplot showing the distribution of tissues (epidermis+cortex+interfascicular fibres (IF), pith, phloem, and xylem) within an inflorescence stem cross-section (I) and barplot showing the interfascicular fibers thickness (J) among the different genotypes. Means ± SE (n ≥ 8 plant for each genotype). Letters indicate statistical difference between genotypes according to an ANOVA and Tukey's comparison post-test.

Fig. 2. Soluble sugars, starch and amino acids accumulate in the main inflorescence stem of multiple *sweet* mutants. Barplots the total soluble sugars, starch and total amino acids content of wild type, *swt11swt12*, *swt16swt17* and quadruple mutants. Least-square means from two independent experiments +/- SE are shown (n=9 for each genotype). Different letters indicate significant difference according to a one-way ANOVA (Tukey's test, $p<0.05$).

Fig. 3. *SWEET* genes modulate plant biomass, yield and nitrogen use efficiency. Barplots showing the dry weight (A) and the C/N ratio (B) in different plant parts (i.e. rosette leaves, total stem and seeds) of wild type, *swt11swt12*, *swt16swt17* and quadruple mutants. Barplots showing the plant nitrogen use efficiency (NUE) (C) and the harvest index (HI) (D) for each genotype. Means +/- SE are shown (n≥5 for each genotype). A one-way ANOVA combined with the Tukey's comparison post-test have been made to compare the different genotypes. The different letters indicate significant difference.

Fig. 4. Nitrogen remobilisation efficiency is partly dependent on *SWEET* genes. Barplots showing the proportion on total ^{15}N in rosette (A), stem (B), and seeds (C) and the N remobilisation efficiency (NRE) (D) in the wild-type, *swt11swt12*, *swt16swt17* and quadruple mutants. (E) Pie charts showing the proportion of N originating from N remobilisation or post-

flowering N uptake in seeds of the wild type, *swt11swt12*, *swt16swt17* and *swt-q* mutants. Means +/- SE are shown (n≥5 for each genotype). A one-way ANOVA combined with the Tukey's comparison post-test have been made to compare the different genotypes. The different letters indicate significant difference.

Fig. 5. Mutation in *SWEET* genes affects the vascular bundle development.
(A) Photograph of the different vascular bundle (VB) types within an inflorescence stem cross-section showing the M-type, B-type and L-type VBs. Scale bar = 100 µm. (B) Stacked histogram showing the number of each VB type in the different genotypes. Values are means ± SD (n=5-6 plants). (C) Heatmap of anatomical traits describing the xylem tissue in M-type, B-type and L-type VBs of the wild type, *swt11swt12*, *swt16swt17*, and *swt-q* mutants. The data are presented as the value of mutant lines over the value of WT plants ratios in different degree of blues for the statistically significant differences. The non-significant differences are presented in white. A one-way ANOVA combined with the Tukey's comparison post-test has been performed on the raw data to compare the genotypes. The results of the ANOVA test are presented beside each VB type and those of the Tukey's comparison post-test are presented in Supplementary Figs. 3, 4 and 5.

Fig. 6. Expression pattern of SWEET11, 12, 16 and 17 in the different vascular bundle types and adjacent tissues. Histochemical analysis of GUS activity in lines expressing SWEET11-GUS (A to C), SWEET12-GUS (D-F), SWEET16-GUS (G-I) or SWEET17-GUS (J-L) fusion proteins driven by their native promoter in sections taken at the bottom of the inflorescence stem after 7-weeks of growth. Photographs are showing GUS expression in M-type vascular bundle (A, D, G and J), in B-type vascular bundle (B, E, H and K) or in L-type vascular bundle (C, F, I and L). Asterisks point to cells showing blue GUS staining in xylem parenchyma cells. Lignin is colored pink after phloroglucinol staining. ep, epidermis; co, cortex; iff, interfascicular fibers; ph, phloem; st: starch sheath cells; xy, xylem.

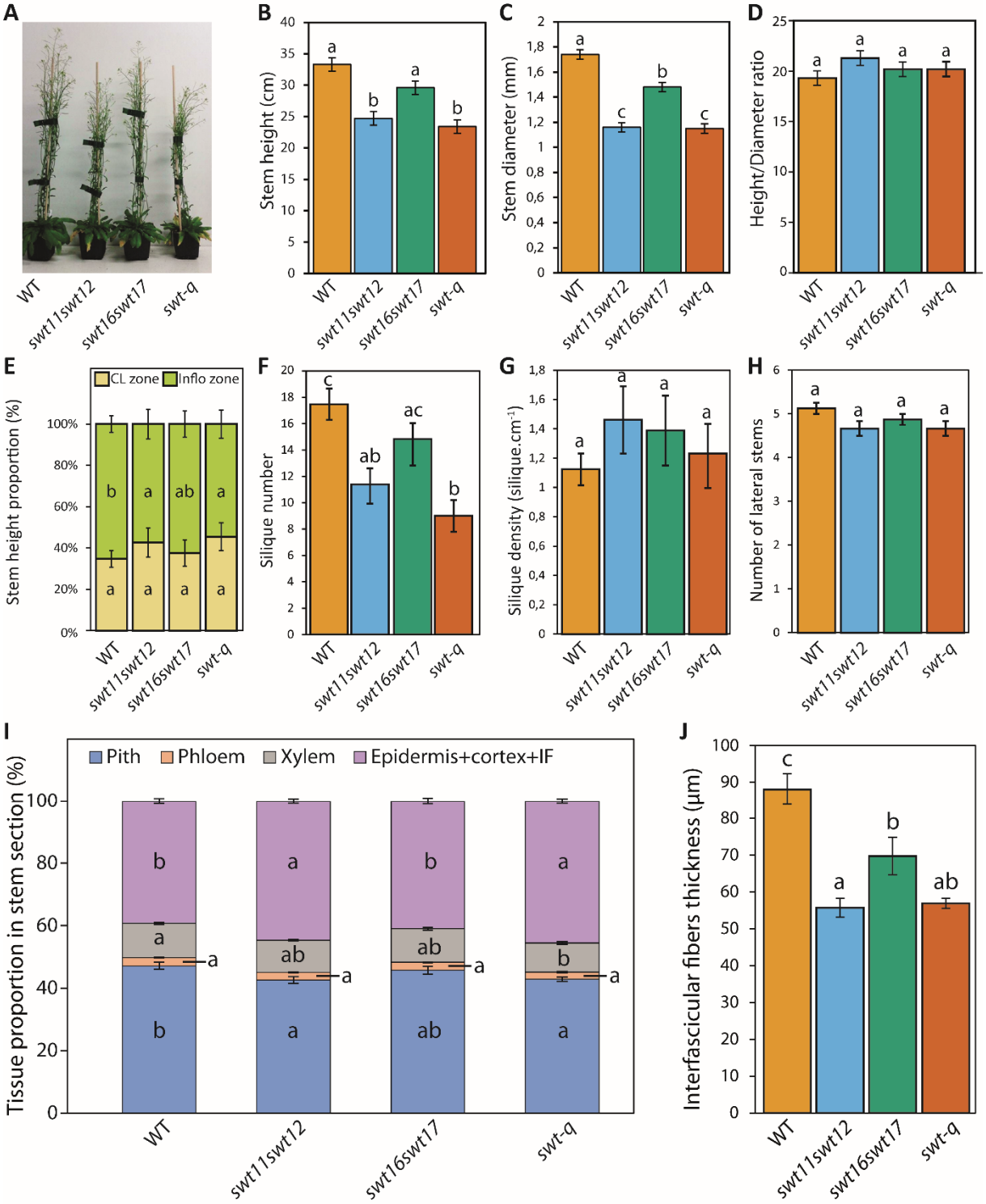

Fig. 1. Main inflorescence growth and development is altered in the quadruple *sweet* mutant line. Photographs of a representative plant of wild-type, *swt11swt12*, *swt16swt17* and quadruple mutants taken at 45 DAS (A). Barplots showing the main inflorescence stem height (B), diameter (C) and the stem height-to-stem diameter ratio (D). Least-square means from three independent cultures ± SE (n=17 for each genotype). Letters indicate statistical difference between genotypes according to an ANOVA and Tukey's comparison post-test. Proportion of

the stem occupied by the “cauline leaf zone” (CL zone) and the “true inflorescence zone” (Inflo zone) (E). Barplots showing the silique number (F), the silique density (G) and the number of lateral inflorescence stems (H). Stacked barplot showing the distribution of tissues (epidermis+cortex+interfascicular fibres (IF), pith, phloem, and xylem) within an inflorescence stem cross-section (I) and barplot showing the interfascicular fibers thickness (J) among the different genotypes. Means ± SE (n ≥ 8 plant for each genotype). Letters indicate statistical difference between genotypes according to an ANOVA and Tukey’s comparison post-test.

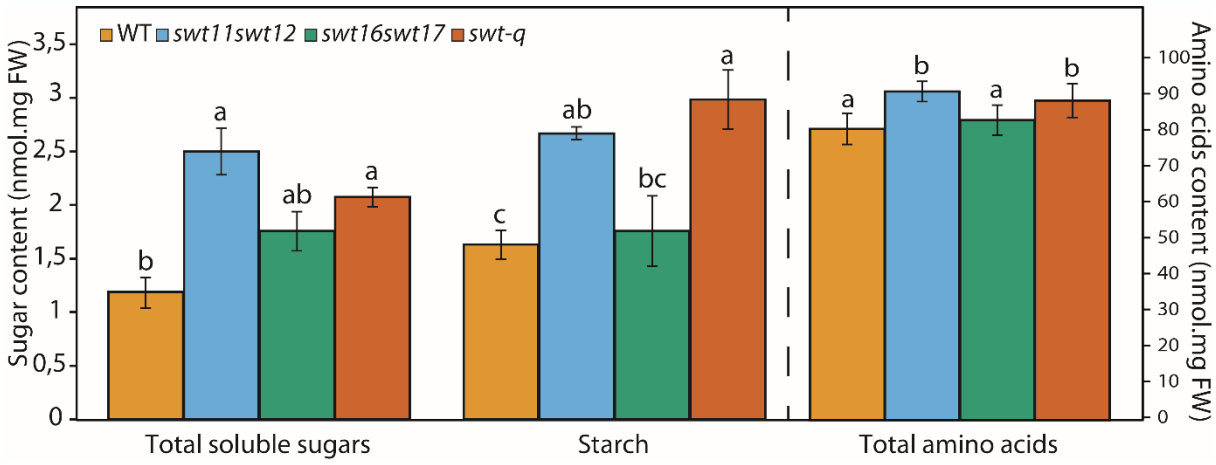

Fig. 2. Soluble sugars, starch and amino acids accumulate in the main inflorescence stem of multiple *sweet* mutants. Barplots the total soluble sugars, starch and total amino acids content of wild type, *swt11swt12*, *swt16swt17* and quadruple mutants. Least-square means from two independent experiments +/- SE are shown (n=9 for each genotype). Different letters indicate significant difference according to a one-way ANOVA (Tukey's test, $p<0.05$).

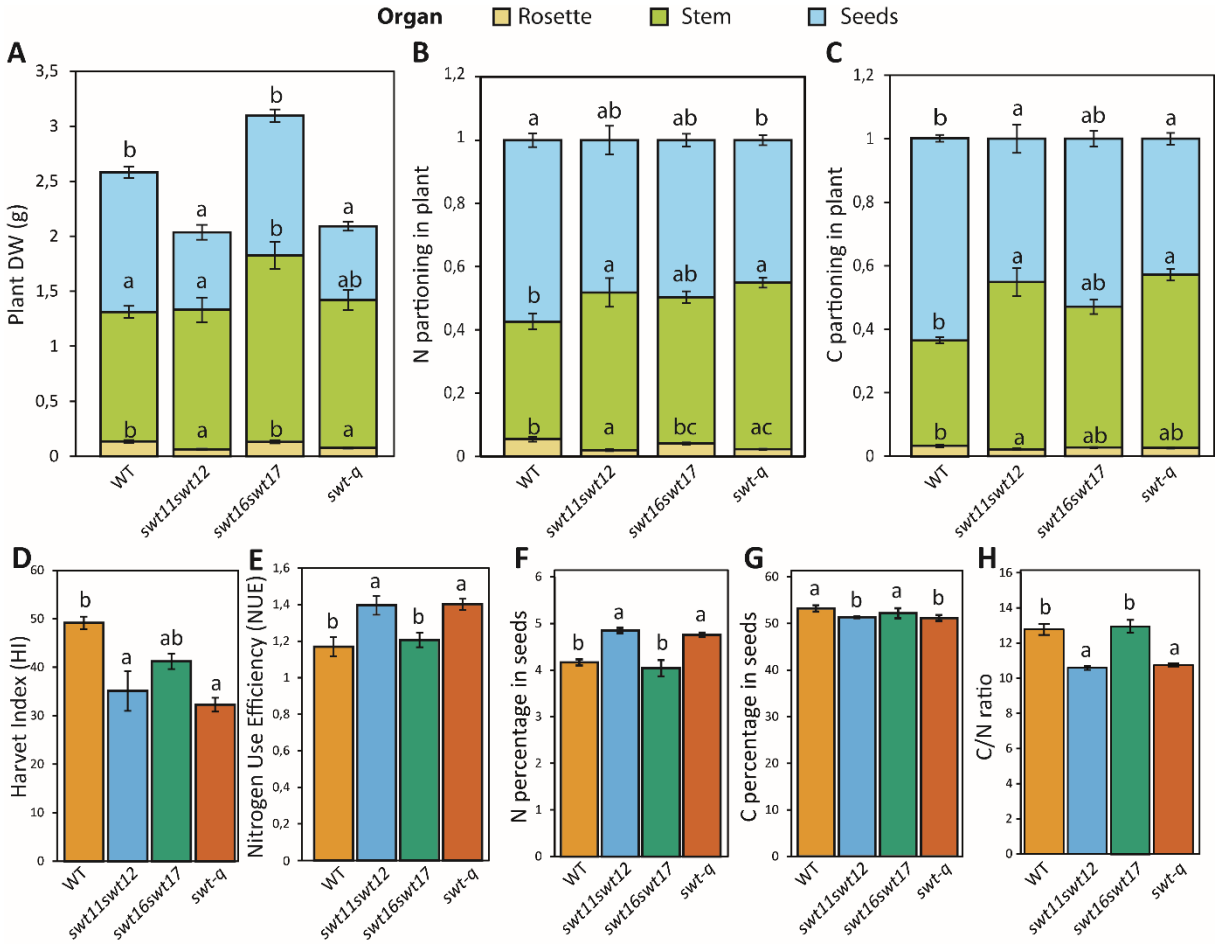

Fig. 3. *SWEET* genes modulate plant biomass, yield and nitrogen use efficiency. Barplots showing the dry weight (A) and the C/N ratio (B) in different plant parts (i.e. rosette leaves, total stem and seeds) of wild type, *swt11swt12*, *swt16swt17* and quadruple mutants. Barplots showing the plant nitrogen use efficiency (NUE) (C) and the harvest index (HI) (D) for each genotype. Means +/- SE are shown (n≥5 for each genotype). A one-way ANOVA combined with the Tukey's comparison post-test have been made to compare the different genotypes. The different letters indicate significant difference.

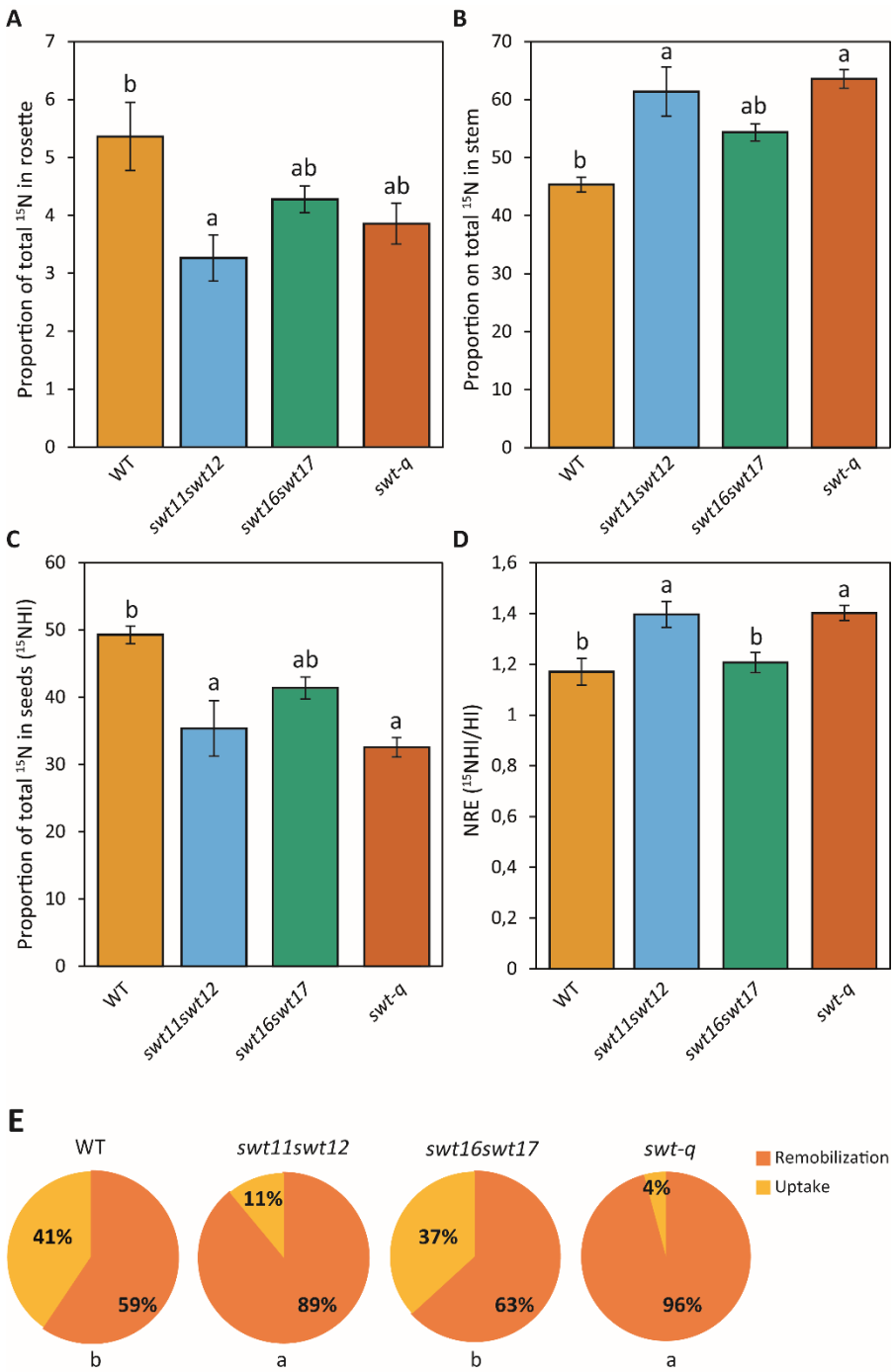

Fig. 4. Nitrogen remobilisation efficiency is partly dependent on *SWEET* genes. Barplots showing the proportion on total ^{15}N in rosette (A), stem (B), and seeds (C) and the N remobilisation efficiency (NRE) (D) in the wild-type, *swt11swt12*, *swt16swt17* and quadruple mutants. (E) Pie charts showing the proportion of N originating from N remobilisation or post-flowering N uptake in seeds of the wild type, *swt11swt12*, *swt16swt17* and *swt-q* mutants. Means +/- SE are shown (n≥5 for each genotype). A one-way ANOVA combined with the Tukey's comparison post-test have been made to compare the different genotypes. The different letters indicate significant difference.

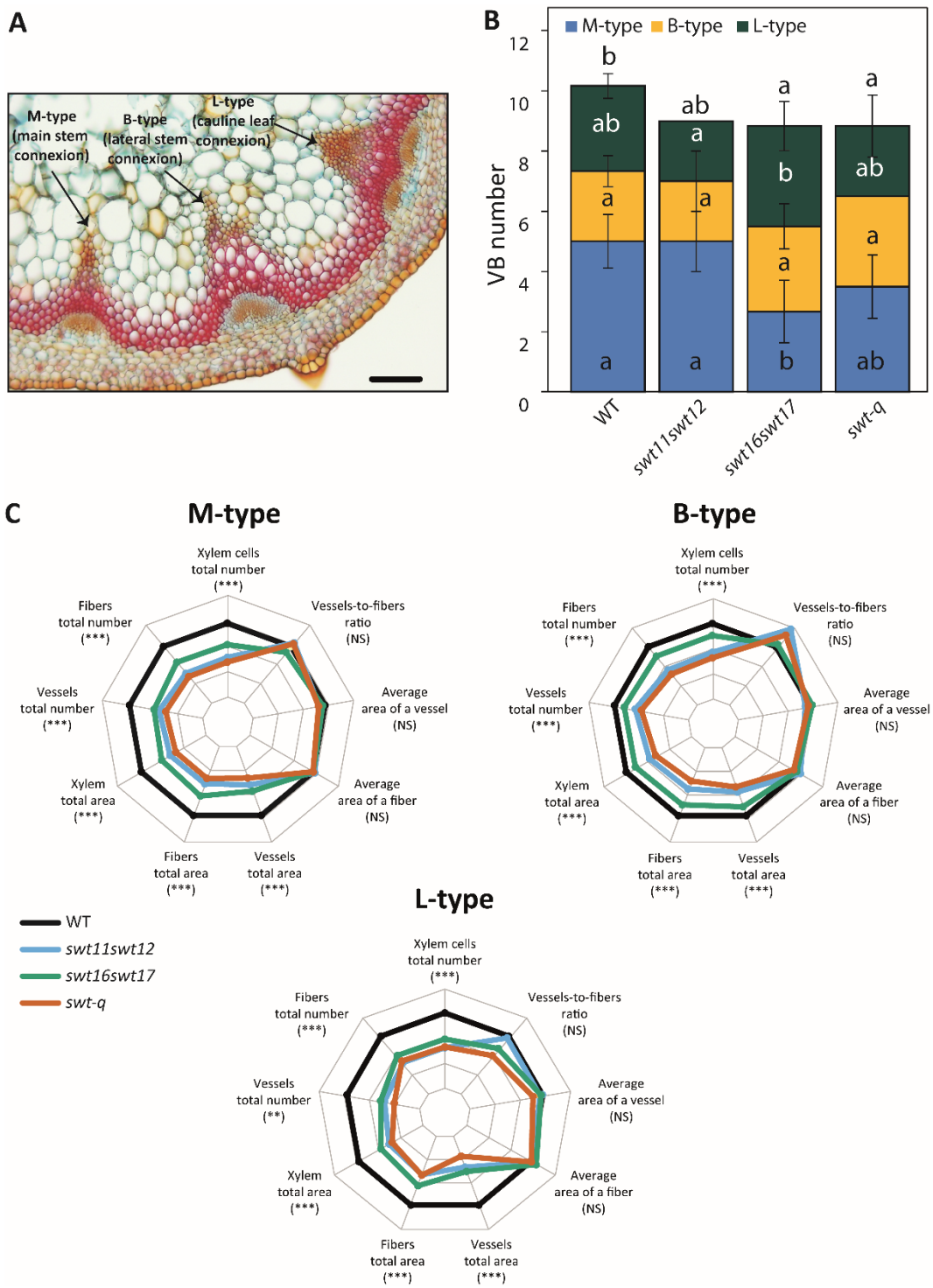

Fig. 5. Mutation in *SWEET* genes affects the vascular bundle development.

(A) Photograph of the different vascular bundle (VB) types within an inflorescence stem cross-section showing the M-type, B-type and L-type VBs. Scale bar = 100 µm. (B) Stacked histogram showing the number of each VB type in the different genotypes. Values are means ± SD (n=5-6 plants). (C) Heatmap of anatomical traits describing the xylem tissue in M-type, B-type and L-type VBs of the wild type, *swt11swt12*, *swt16swt17*, and *swt-q* mutants. The data are presented as the value of mutant lines over the value of WT plants ratios in different degree

of blues for the statistically significant differences. The non-significant differences are presented in white. A one-way ANOVA combined with the Tukey's comparison post-test has been performed on the raw data to compare the genotypes. The results of the ANOVA test are presented beside each VB type and those of the Tukey's comparison post-test are presented in Supplementary Figs. 3, 4 and 5.

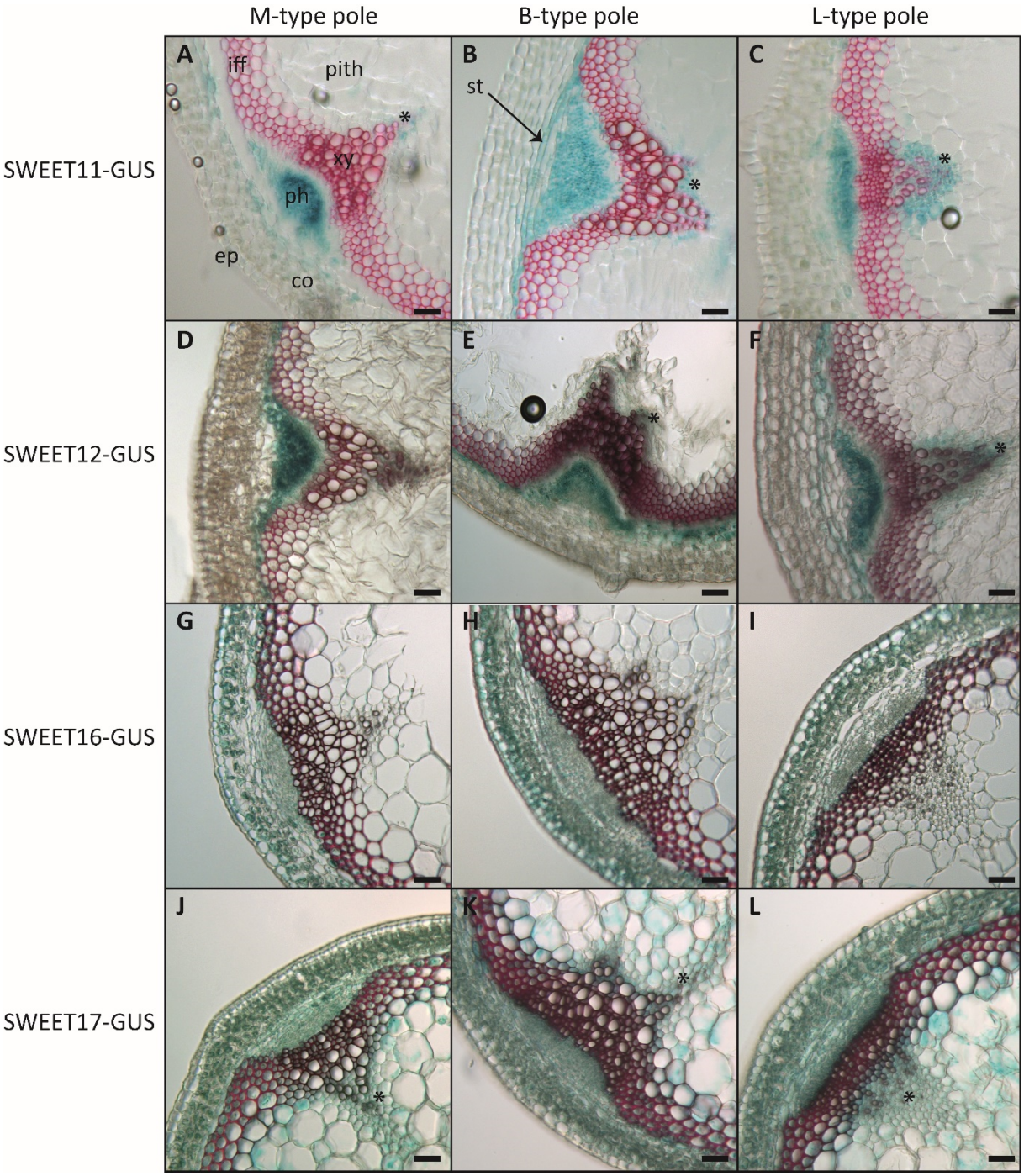

Fig. 6. Expression pattern of SWEET11, 12, 16 and 17 in the different vascular bundle types and adjacent tissues. Histochemical analysis of GUS activity in lines expressing SWEET11-GUS (A to C), SWEET12-GUS (D-F), SWEET16-GUS (G-I) or SWEET17-GUS (J-L) fusion proteins driven by their native promoter in sections taken at the bottom of the inflorescence stem after 7-weeks of growth. Photographs are showing GUS expression in M-type vascular bundle (A, D, G and J), in B-type vascular bundle (B, E, H and K) or in L-type vascular bundle (C, F, I and L). Asterisks point to cells showing blue GUS staining in xylem

parenchyma cells. Lignin is colored pink after phloroglucinol staining. ep, epidermis; co, cortex; iff, interfascicular fibers; ph, phloem; st: starch sheath cells; xy, xylem.